Probing the Mechanism of Hamster Arylamine *N*-Acetyltransferase 2 Acetylation by Active Site Modification, Site-Directed Mutagenesis, and Pre-Steady State and Steady State Kinetic Studies†

Haiqing Wang, Gregory M. Vath, Kara J. Gleason, Patrick E. Hanna, and Carston R. Wagner*

Department of Medicinal Chemistry, College of Pharmacy, University of Minnesota, Minneapolis, Minnesota 55455

Received February 6, 2004; Revised Manuscript Received April 20, 2004

ABSTRACT: Arylamine *N*-acetyltransferases (NATs) catalyze an acetyl group transfer from acetyl coenzyme A (AcCoA) to arylamines, hydrazines, and their N-hydroxylated arylamine metabolites. The recently determined three-dimensional structures of prokaryotic NATs have revealed a cysteine protease-like Cys-His-Asp catalytic triad, which resides in a deep and hydrophobic pocket. This catalytic triad is strictly conserved across all known NATs, including hamster NAT2 (Cys-68, His-107, and Asp-122). Treatment of NAT2 with either iodoacetamide (IAM) or bromoacetamide (BAM) at neutral pH rapidly inactivated the enzyme with second-order rate constants of 802.7 ± 4.0 and 426.9 ± 21.0 M^{-1} s^{-1}, respectively. MALDI-TOF and ESI mass spectral analysis established that Cys-68 is the only site of alkylation by IAM. Unlike the case for cysteine proteases, no significant inactivation was observed with either iodoacetic acid (IAA) or bromoacetic acid (BAA). Pre-steady state and steady state kinetic analysis with *p*-nitrophenyl acetate (PNPA) and NAT2 revealed a single-exponential curve for the acetylation step with a second-order rate constant of (1.4 ± 0.05) × 10^5 M^{-1} s^{-1}, followed by a slow linear rate of (7.85 ± 0.65) × 10^{-3} s^{-1} for the deacetylation step. Studies of the pH dependence of the rate of inactivation with IAM and the rate of acetylation with PNPA revealed similar pK_{a1} values of 5.23 ± 0.09 and 5.16 ± 0.04, respectively, and pK_{a2} values of 6.95 ± 0.27 and 6.79 ± 0.25, respectively. Both rates reached their maximum values at pH 6.4 and decreased by only 30% at pH 9.0. Kinetic studies in the presence of D_2O revealed a large inverse solvent isotope effect on both inactivation and acetylation of NAT2 [$k^{H}_{inact}/k^{D}_{inact}$ = 0.65 ± 0.02 and $(k_2/K_m^{acetyl})^{H}/(k_2/K_m^{acetyl})^{D}$ = 0.60 ± 0.03], which were found to be identical to the fractionation factors (Φ) derived from proton inventory studies of the rate of acetylation at pL 6.4 and 8.0. Substitution of the catalytic triad Asp-122 with either alanine or asparagine resulted in the complete loss of protein structural integrity and catalytic activity. From these results, it can be concluded that the catalytic mechanism of NAT2 depends on the formation of a thiolate−imidazolium ion pair (Cys-S^-−His-ImH^+). However, in contrast to the case with cysteine proteases, a pH-dependent protein conformational change is likely responsible for the second pK_a, and not deprotonation of the thiolate−imidazolium ion. In addition, substitutions of the triad aspartate are not tolerated. The enzyme appears, therefore, to be engineered to rapidly form a stable acetylated species poised to react with an arylamine substrate.

Arylamine *N*-acetyltransferases (NATs,[1] EC 2.3.1.5) catalyze the AcCoA-dependent acetylation of a variety of aromatic amines, hydrazines, and hydrazides. NATs are also capable of catalyzing the formation of highly reactive electrophiles by acetylating the hydroxyl group of arylhydroxylamines and by converting arylhydroxamic acids to *N*-acyloxy esters (*1*−*3*). The NATs are a ubiquitous family of enzymes and have been isolated and cloned from a variety of bacterial, avian, and mammalian tissues. Because many of the substrates for NATs are drugs and environmental xenobiotics, there has been an extensive effort to quantify the potential toxicological risks of exposure to these agents by genetic and epidemiological studies of NAT polymorphisms (*4*). The reaction of NAT-generated electrophiles, thus leading to DNA adduct formation, is believed to be a predominant mechanism responsible for the mutagenic and carcinogenic effects associated with exposure to arylamines (*2*).

† This work was supported by U. S. Public Health Service Grant CA55334 from the National Cancer Institute and a Development Grant in Drug Design from the Department of Medicinal Chemistry, University of Minnesota.

* To whom correspondence should be addressed: Department of Medicinal Chemistry, University of Minnesota, 8-101 Weaver-Densford Hall, 308 Harvard St., Minneapolis, MN 55455. E-mail: wagne003@tc.umn.edu.

[1] Abbreviations: AcCoA, acetylcoenzyme A; BAA, bromoacetic acid; BAM, bromoacetamide; BSA, bovine serum albumin; DMAB, 4-(dimethylamino)benzaldehyde; DTT, dithiothreitol; EDTA, ethylenediaminetetraacetic acid; ESI, electrospray ionization; IAA, iodoacetic acid; IAM, iodoacetamide; IPTG, isopropyl β-D-thiogalactopyranoside; MALDI-TOF, matrix-assisted laser desorption ionization time-of-flight; NAT, arylamine *N*-acetyltransferase; NAT1, hamster monomorphic *N*-acetyltransferase; NAT2, hamster polymorphic *N*-acetyltransferase; PABA, *p*-aminobenzoic acid; PAGE, polyacrylamide gel electrophoresis; PE buffer, potassium phosphate buffer; PMSF, phenylmethanesulfonyl fluoride; PTP, protein tyrosine phosphatase; PNPA, *p*-nitrophenyl acetate; SDS, sodium dodecyl sulfate; SKIE, solvent kinetic isotope effect; *St*NAT, *S. typhimurium* NAT; TCA, trichloroacetic acid.

10.1021/bi0497244 CCC: $27.50
Published on Web 06/03/2004

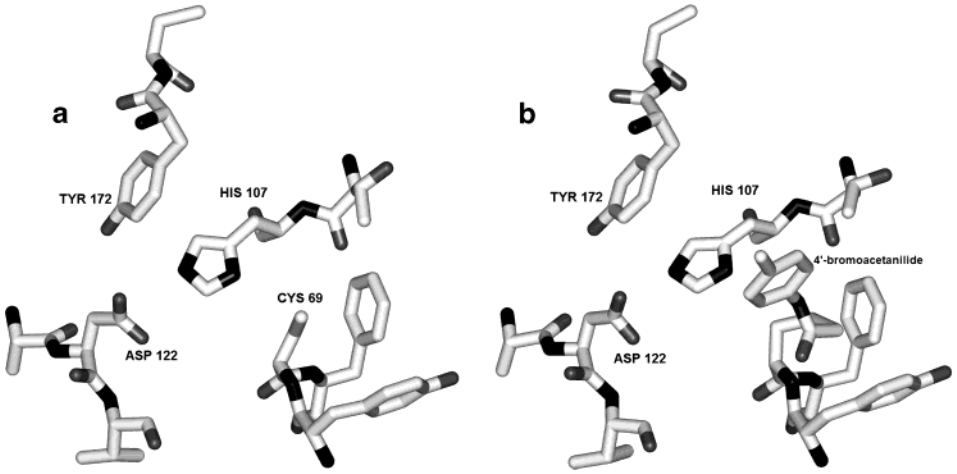

FIGURE 1: X-ray crystallographic structure of the *St*NAT active site (a) without bound 4′-bromoacetanilide or (b) with bound 4′-bromoacetanilide (*8*).

Steady state kinetic studies have revealed that NATs catalyze acetyl transfer by a classical ping-pong kinetic mechanism (*1*, *3*). Affinity labeling studies of hamster NAT demonstrated that an essential cysteine was necessary for catalytic activity and that inactivation of the enzyme could be prevented by preincubation with AcCoA (*5*). Site-directed mutagenesis studies of human NAT2 and *Salmonella typhimurium* NAT (*St*NAT) revealed that Cys-68 and Cys-69, respectively, were likely the residues responsible for mediating acetyl group transfer (*6*, *7*). Recently, the X-ray structures of the apo and affinity-labeled *St*NAT and *Mycobacterium smegmatis* NAT were determined and revealed a catalytic triad consisting of Cys-69, His-107, and Asp-122, reminiscent of cysteine proteases and factor XIII transglutaminase (Figure 1a) (*8*, *9*). Three-dimensional homology modeling studies of human NAT1 and NAT2, based on the *St*NAT structure, have demonstrated that the enzymes contain identical catalytic triads (*10*, *11*). This result is consistent with the strict conservation of these three residues across the NAT superfamily (Figure 1b) (*12*, *13*). Similar modeling studies have been conducted with hamster NAT1 and NAT2 and are fully consistent with the results obtained for the human enzyme (G. Vath and C. R. Wagner, unpublished results).

The role of the active site histidine in cysteine-dependent proteases has been extensively investigated by pH-dependent alkylation and steady state experiments. In general, because the pK_a of the enzyme active site cysteine has been found to be acidic, the histidine has been thought to be responsible for activating the cysteinyl sulfhydryl moiety by formation of a thiolate−imidazolium ion pair (*14*−*18*). Since the catalytic triad of NATs also contains a histidine, it is likely that formation of a thiolate−imidazolium ion pair is a necessary prerequisite for catalysis. However, a rationale for NAT catalysis that is based on cysteine protease catalysis is not entirely apparent given the likely hydrophobic active site environment, as well as the strictly conserved triad aspartate. Because enzyme acetylation occurs prior to substrate acetylation, we have chosen to characterize the reactivity of hamster NAT2 Cys-68 with thiol specific active site labels. Enzyme acetylation was examined by single-turnover kinetics and the importance of proton transfer during the catalysis determined by solvent kinetic isotope effect studies. In addition, the role of the conserved triad aspartate was probed by site-directed mutagenesis.

EXPERIMENTAL PROCEDURES

Materials. Ammonium sulfamate, PABA, *N*-1-naphthylethylenediamine dihydrochloride, IAM, BAM, IAA, BAA, ampicillin, pepsin, 3,3-dimethylglutaric acid, D_2O, NaOD, and DCl were purchased from Sigma-Aldrich (St. Louis, MO). AcCoA and PD-10 desalting columns were purchased from Amersham Biosciences (Piscataway, NJ). All other reagents were purchased from Fisher Scientific, Inc. (Chicago, IL). Spectrophotometric data were collected on a Varian (Palo Alto, CA) Cary 50 UV−vis spectrophotometer. Transient kinetic data were collected on a single-wavelength stopped flow apparatus (Applied Photophysics, model SX.18MV). rpHPLC was conducted with a Beckman/Coulter Gold System and Karat 32 software. A QuickChange site-directed mutagenesis kit was purchased from Stratagene (La Jolla, CA). A protein refolding kit was purchased from Novagen (Madison, WI).

Expression and Purification of Wild-Type NAT2. NAT2 was expressed and purified as described previously (*19*) with some modifications. An ion exchange column (50 mm diameter) packed with Q-Sepharose fast flow beads (Pharmacia, 60 mL) was used to separate the NAT2−dihydrofolate reductase (DHFR) fusion protein from the supernatant. A MonoQ column (HR 10/10, Pharmacia) was used to separate NAT2 from DHFR after thrombin cleavage. Both columns were attached to a Pharmacia FPLC system with an LCC 500 plus system controller, two P500 solvent delivery pumps, a UV monitor (model 2151), and a P500 collector. The columns were eluted with 80 mL of 20 mM potassium phosphate (PE) buffer [with 1 mM EDTA and 1 mM DTT (pH 7.4)], followed by 600 mL of a 0 to 0.4 M KCl gradient in PE buffer. Fractions (10 mL) were collected at a flow rate of 1−2 mL/min at 4 °C. The NAT2−DHFR fusion protein eluted from the Q-Sepharose column at 0.26 M KCl, while NAT2 eluted from the MonoQ column at 0.08 M KCl. The homogeneous recombinant protein was stored at −80 °C as a 10% glycerol/PE solution. Protein concentrations were determined with the Bradford protein assay (*20*).

Site-Directed Mutagenesis. Site-directed mutagenesis of NAT2 catalytic triad Asp-122 to Asn (D122N) or Ala (D122A) was carried out with the pPH70D vector and QuickChange site-directed mutagenesis kit (Stratagene). The oligonucleotide primer used for D122N was 5′-GAT AGG

AAC TAC ATT GTT AAT GCT GGG TTT GGA CGT TCC-3′ and for D122A 5′-GAT AGG AAC TAC ATT GTT GCT GCT GGG TTT GGA CGT TCC-3′. Mutant DNA was fully sequenced by automated sequencing, thus ensuring that no additional mutations had been incorporated. The mutated plasmids were transformed into BL-21 Codon Plus (RIL) *Escherichia coli* cells according to the supplier's instructions.

Expression and Purification of D122A and D122N Mutant Proteins. The expression levels of D122N and D122A mutant proteins were tested under different growth conditions. Overnight cultures (100 mL) were grown from single colonies, and 10 mL of the cultures was inoculated into 1 L of LB medium containing ampicillin (final concentration of 100 μg/mL) and chloramphenicol (final concentration of 50 μg/mL). Cultures were grown aerobically at 37 or 25 °C to an OD_{600} of 0.4 or 1.0, at which time IPTG was added to a final concentration of 200 μM. After incubation for an additional 1−5 h, the cells were harvested by centrifugation at 5000*g* for 15 min at 4 °C. The cells were lysed as previously described (*19*). The mutant proteins in the inclusion bodies were resolubilized with a protein refolding kit (Novagen). More than 90% of the mutant proteins were resolubilized after extensive dialysis in 20 mM Tris buffer [with 1 mM DTT (pH 8.0)] and DEAE column purification. Control experiments were conducted under the same conditions with the insoluble protein generated during the expression of wild-type NAT2.

Mutant Protein Assays. The overexpression levels of the mutants in soluble fractions and inclusion bodies were checked by SDS−PAGE and immunoblots with goat anti-FLAG M2 monoclonal antibody (VWR) (*19*).

NAT2 Activity Assay. AcCoA-dependent acetylation of PABA was performed at 37 °C as described previously (*19*). NAT2 was preincubated with AcCoA in sodium pyrophosphate buffer (116.7 μL, 50 mM, pH 7.0; 1 mM DTT) for 1 min, and the reaction was initiated by addition of PABA (50 μL). The final assay mixture contained NAT2 (0.5 μg/mL, 14.6 nM), AcCoA (0.6 mM), and PABA (0.1 mM). After the mixture had been incubated for 2 min, the reaction was terminated by adding ice-cold TCA [5% (w/v) in H_2O, 333 μL]. The reaction rate was determined by diazotization of the unacetylated PABA according to the Bratton−Marshall procedure (*19*, *21*). The absorbance was read at 540 nm. Activity was expressed as the micromoles of PABA acetylated per milligram of protein per minute. The assays for the mutant proteins were carried out as described above, except the concentration of protein extracts was 50 μg/mL and the incubation time was prolonged to 15 min.

Inactivation of NAT2 by Iodoacetamide (IAM) or Bromoacetamide (BAM). Incubation mixtures contained NAT2 (26.7 μg/mL, 0.78 μM), IAM (or BAM, 20−80 μM), and 50 mM sodium pyrophosphate buffer [with 80 mM NaCl, 0.1 mM DTT, and 1% glycerol (pH 7.0)] in a total volume of 200 μL. Incubations were conducted at 25 °C. The reaction was initiated by addition of IAM (or BAM) dissolved in H_2O (10 μL). Aliquots (2.5 μL) were withdrawn at 15 s intervals (from 15 to 90 s) and added to the activity assay mixture containing AcCoA dissolved in the reaction buffer (114.2 μL). After incubation for 1 min, the activity assay was initiated by addition of PABA (50 μL). The final assay mixture contained NAT2 (0.4 μg/mL, 11.7 nM), AcCoA (0.6 mM), PABA (0.1 mM), and diluted residual IAM (or BAM, 0.3−1.2 μM). The assay was carried out at 37 °C as described above. The percentage of activity remaining after incubation with IAM (or BAM) was calculated with respect to controls which contained DMSO, but not IAM (or BAM). Inactivation data were plotted as ln % remaining activity ($[E]/[E]_t$) versus time (t) (Scheme 1, eq 1). The second-order rate constant (k_{inact}) was obtained by plotting $(k_{inact})_{obs}$ versus inhibitor concentration (eq 2). The reaction order (n) was obtained from the slope of eq 3.

Scheme 1

$$\mathrm{NAT2 + n\,I \xrightarrow{k_{inact}} NAT2\text{-}I_n}$$

$$\mathrm{Ln}[E]/[E]_t = -(k_{inact})_{obs} \times t \quad (1)$$

$$(k_{inact})_{obs} = k_{inact} \times [I]_0^n \quad (2)$$

$$\log (k_{inact})_{obs} = n\log[I]_0 + \log k_{inact} \quad (3)$$

Inactivation of NAT2 by Iodoacetic Acid (IAA) or Bromoacetic Acid (BAA). To NAT2 (5.34 μg) in sodium pyrophosphate buffer [190 μL, 50 mM; with 80 mM NaCl, 0.1 mM DTT, and 1% glycerol (pH 7.0)] was added iodoacetic acid (IAA) or bromoacetic acid (BAA) dissolved in H_2O (10 μL). The final concentration of NAT2 was 26.7 μg/mL (0.78 μM) and that of IAA 2 mM (or 3 mM for BAA). Incubations were carried out for 80 min at 37 °C. At 5−10 min intervals, the remaining NAT2 activity was assayed as described in IAM and BAM inactivation studies. The percentage of activity remaining after incubation with IAA (or BAA) was calculated with respect to controls that contained H_2O, but not IAA (or BAA).

Prevention of Iodoacetamide Inactivation of NAT2 by AcCoA. NAT2 (44.5 μg/mL, 1.3 μM) was incubated with AcCoA (0−20 μM) for 1 min in 50 mM sodium pyrophosphate buffer [with 0.1 mM DTT (pH 7.0)] at 37 °C. IAM (final concentration of 2 μM) was added, and incubation was continued for an additional 10 min. Reactions were terminated by transferring the mixture to a Sephadex G-25 PD-10 gel filtration column, followed by the addition of incubation buffer (2.4 mL). The protein was eluted with 2 mL of the buffer, and the NAT2 activity was determined as described above. Percent residual activity for each experiment was calculated on the basis of the control experiment in which IAM was omitted from the incubation mixture.

Ionic Strength Dependence of Iodoacetamide Inactivation of NAT2. Incubation of NAT2 (44.5 μg/mL, 1.3 μM) with IAM (20 μM) was carried out at 37 °C in 3,3-dimethylglutaric acid [200 μL, 50 mM, with 0.1 mM DTT and 1 mM EDTA (pH 7.0)]. The ionic strength of the buffer was adjusted to a range of 0.6−0.98 M with NaCl. After incubation for 1 min, the reaction mixture was loaded onto a PD-10 gel filtration column. The NAT2 activity was determined as described above.

pH Profile of Iodoacetamide Inactivation. NAT2 (26.7 μg/mL, 0.78 μM) was incubated with IAM (25 μM) in either 50 mM 3,3-dimethylglutaric acid buffer [with 0.1 mM DTT and 1% glycerol (pH 5.0−7.2)] or 50 mM Tris buffer [with 0.1 mM DTT and 1% glycerol (pH 7.5−9.0)] at 25 °C. The ionic strength was maintained at 150 mM with NaCl. Aliquots (6 μL) were withdrawn at 15 s intervals (15−90 s)

Scheme 2

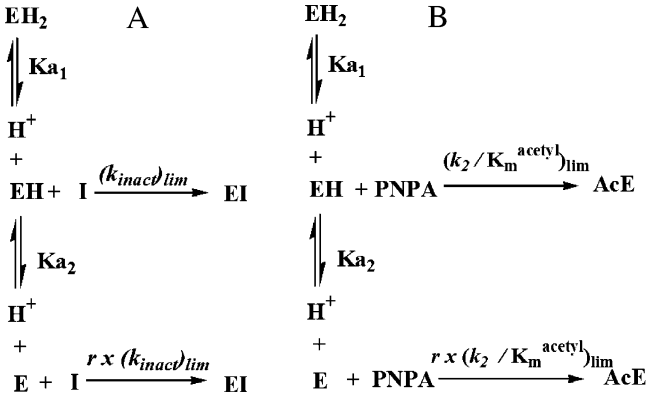

$$\frac{k_{inact}}{(k_{inact})_{lim}} = \frac{1 + r\,x\,10^{(pH-pKa2)}}{1 + 10^{(pH-pKa2)} + 10^{(pKa1-pH)}} \quad (4a)$$

$$\frac{k_2/K_m^{acetyl}}{(k_2/K_m^{acetyl})_{lim}} = \frac{1 + r\,x\,10^{(pH-pKa2)}}{1 + 10^{(pH-pKa2)} + 10^{(pKa1-pH)}} \quad (4b)$$

and transferred to an assay tube containing AcCoA and PABA in 3,3-dimethylglutaric acid buffer [194 μL, 50 mM; with 80 mM NaCl and 1 mM DTT (pH 7.0)]. The final assay mixture contained AcCoA (500 μM), PABA (40 μM), NAT2 (1.6 μg/mL), and remaining IAM (0.75 μM). After the mixture had been incubated for 100 s, the reaction was terminated by the addition of TCA [40% (w/v), 50 μL], followed by dimethylaminobenzaldehyde (DMAB) dissolved in 90% acetonitrile [250 μL, 5% (w/v)]. The remaining PABA concentration was quantified by reaction with DMAB (*22*), which gave a maximum absorbance at 450 nm (ϵ_{450} = 15 900 M^{-1} cm^{-1}). The control activity ranged from 22 to 27 μmol mg^{-1} min^{-1} over the pH range. The results represent the average of duplicate experiments. The theoretical line (Figure 5) was created by fitting the data to eq 4a, according to a mechanism involving three protonic states, only two (EH and E) of which can undergo the reaction (Scheme 2A). The inactivation rate constants for EH and E were represented as $(k_{inact})_{lim}$ and $(k_{inact})_{lim}'$, respectively, where $(k_{inact})_{lim}' = r(k_{inact})_{lim}$ when $r < 1$. The JMP IN software suite (SAS Institute, Inc.) was used for nonlinear regression curve fitting.

Solvent Kinetic Isotope Effects. Solvent kinetic isotope effects on iodoacetamide inactivation (k_{inact}) were determined at pL 6.4 and 9.0. The inactivation reactions were conducted essentially as described for the pH-dependent studies. For pL 6.4, 3,3-dimethylglutaric acid buffer was used, and for pL 9.0, Tris buffer was used. The inactivation reaction mixtures in D_2O contained 95% D_2O. The pD was measured using the empiric relation pD = pH meter reading + 0.4 (*23*) and adjusted with DCl or NaOD. The results represent the average of two experiments. Solvent kinetic isotope effects were calculated as the ratio of k_{inact} values obtained from H_2O and from 95% D_2O.

Pre-Steady State Kinetics. Single-turnover reactions of NAT2 acetylation were performed at 25 °C using a single-wavelength stopped flow apparatus (Applied Photophysics, model SX.18MV) equipped with a constant-temperature circulating water bath. NAT2 (276 μg/mL, 8 μM) in MOPS

Scheme 3

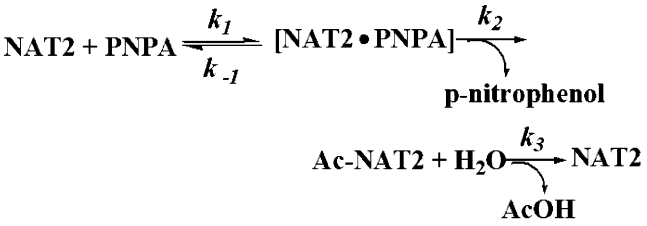

$$P(t) = A\,(1 - e^{-k_{obs}t}) \quad (5)$$

$$k_{obs} = k_2[PNPA]/(K_m^{acetyl} + [PNPA]) \quad (6)$$

$$K_m^{acetyl} = (k_2 + k_{-1})/k_1 \quad (7)$$

when $K_m^{acetyl} >> [PNPA]$

$$k_{obs} = (k_2/K_m^{acetyl})\,[PNPA] \quad (8)$$

$$\frac{V}{[E]_{total}} = \frac{k_{cat}\,[PNPA]}{K_m + [PNPA]} \quad (9)$$

$$K_m = K_m^{acetyl} \times \frac{k_3}{k_2 + k_3} \quad (10)$$

$$k_{cat} = \frac{k_2 k_3}{k_2 + k_3} \quad (11)$$

$$\frac{[E]_{total}}{V} = \underbrace{\frac{K_m^{acetyl}}{k_2\,[PNPA]} + \frac{1}{k_2}}_{\frac{1}{k_{obs}}} + \frac{1}{k_3} \quad (12)$$

$$t_{1/2} = \frac{Ln\ 2}{k_{cat}} \quad (13)$$

buffer [1 mL, 100 mM; with NaCl 150 mM (pH 7.0)] was transferred to one stopped flow syringe. PNPA (160−3000 μM) in MOPS buffer [1 mL, 100 mM; with 150 mM NaCl and 3% DMSO (pH 7.0)] was added to the second stopped flow syringe. Equal volumes (50 μL) of the enzyme solution and substrate were mixed rapidly. The release of *p*-nitrophenol [$P_{(t)}$] was monitored at 400 nm. Single-turnover progress curves were fitted with eq 5 using JMP software, where *A* is the amplitude and k_{obs} is the pseudo-first-order rate constant for the acetylation step (Scheme 3). The results represent the average of three experiments. The kinetic parameter k_2/K_m^{acetyl} was obtained by plotting k_{obs} versus PNPA concentration (eq 8).

pL Profiles of NAT2 Single Turnover with PNPA. Stopped flow kinetic experiments were performed with NAT2 (final concentration of 4 μM) and PNPA (final concentration of 320 μM) in a pL range of 5.2−9.0. Buffers were prepared in H_2O and D_2O in parallel, and the pD values for the D_2O buffers were corrected according to the formula pD = pH meter reading + 0.4 (*23*). The pD values of the buffers were adjusted with DCl and NaOD. For the pL range from 5 to 7.2, 3,3-dimethylglutaric acid (50 mM) was used; for the pL range from 7.5 to 9.0, Tris buffer (50 mM) was used. The ionic strength was maintained at 150 mM with NaCl. Reaction mixtures in D_2O buffer contained 95% D_2O. For pL values ranging from 6.4 to 9, the reaction was monitored

at 400 nm, and for pL values from 5.0 to 6.0, reactions were monitored at 340 nm. The results represent the average of triplicate experiments. The theoretical lines (Figure 9) were created by fitting the data to eq 4b, which shares the same mechanism as eq 4a (Scheme 2B).

Proton Inventory Studies of NAT2 Acetylation with PNPA. Buffer solutions with different deuterium atom fractions *n* were prepared gravimetrically by mixing appropriate quantities of dimethylglutaric acid buffers made in H_2O and D_2O. The experiments were performed under two pL conditions, 6.4 and 8.0, with essentially the same methodology as described for the pre-steady state kinetic studies. The results represent the average of three experiments. The experimental data were fitted to eq 14 (*23*), where k_0 is the pseudo-first-order rate constant in H_2O, k_n is the pseudo-first-order rate constant in the *n* mole fraction of D_2O, ϕ_i^T and ϕ_j^R are the isotopic fractionation factors of the *i*th transition state proton and *j*th reactant state proton, respectively.

$$\frac{k_n}{k_0} = \frac{\prod(1 - n + n\phi_i^{T})}{\prod(1 - n + n\phi_j^{R})} \quad (14)$$

Steady State Kinetics of Acetyl-Enzyme Hydrolysis. The incubation mixture contained NAT2 (final concentrations of 4 and 8 μM), PNPA (final concentration of 320 μM), and MOPS buffer [100 mM; with 150 mM NaCl (pH 7.0) and 0.1 mM DTT] in a total volume of 500 μL. The reaction was initiated by addition of PNPA dissolved in DMSO (5 μL). The reaction was carried out at 25 °C. Reaction rates were determined by measuring the increase in absorbance at 400 nm. Control experiments were performed without the enzyme. The results represent the average of three experiments. The slope of the line (Figure 8) is the acetyl-enzyme hydrolysis velocity (*V*). Equation 9 was transformed to eq 12 by substituting k_{cat} and K_m with k_2, k_3, and K_m^{acetyl} (eqs 10 and 11). The acetyl-enzyme hydrolysis rate constant, k_3, was determined by fitting the data to eq 12, where $[E]_{total}$ is the total enzyme concentration in the experiments and k_{obs} is the pseudo-first-order rate constant for the acetylation step (eq 8). The half-life of the acylenzyme ($t_{1/2}$) was calculated from eq 13.

ESI-Mass Spectrometry of NAT2 Treated with Iodoacetamide. NAT2 (2 mg/mL, 58 μM) was incubated with IAM (final concentration of 120 μM) in 20 mM potassium phosphate buffer [with 10% glycerol, 1 mM EDTA, and 0.1 mM DTT (pH 7.4)] in a final volume of 100 μL. After incubation for 5 min at 25 °C, which resulted in a greater than 90% loss of activity, the reaction was terminated by adding 10% acetic acid (25 μL) and 1% TFA (1.25 μL). The sample was centrifuged at 16000*g* for 5 min and was subjected to rpHPLC on a Vydac C4 MS column (model 214MS, 4.6 mm × 250 mm and guard column). A stepwise isocratic elution with a flow rate of 1 mL/min was used. Solvent A was 2.5% (v/v) acetonitrile in 0.01% (v/v) trifluoroacetic acid, and solvent B was 90% acetonitrile in 0.01% trifluoroacetic acid. The column was eluted with 0% B (2 min), 35% B (4 min), 65% B (5 min), and 100% B (10 min). A sample of NAT2 that had not been treated with IAM was prepared by the same protocol. NAT2 eluted at approximately 10.0 min. The protein-containing fractions were stored at −80 °C.

Protein masses were obtained with a Thermo-Finnigan LCQ Classic electrospray ion trap mass spectrometer by direct infusion. Instrument settings were as follows: heated capillary temperature of 200 °C, spray voltage of 4.5 kV, sample flow rate of 5 μL/min, and nitrogen sheath gas of 60 units. Centroid data were collected in the positive ion mode. The multiply charged ion envelope (*m*/*z* 700−2000) was analyzed with the deconvolution tools in the XCALIBUR software suite. The addition of one acetamido group was expected to increase the mass by 57 Da.

Pepsin Digestion of NAT2 Modified with IAM and MS Sequencing of the IAM-Modified Peptide. The inactivation conditions were identical with those described above. After incubation for 5 min, the reaction mixture was loaded onto a Sephadex G-25 PD-10 column that had been equilibrated with sodium pyrophosphate buffer (5 mM, pH 7.0), and the protein was eluted with the same buffer. The pH of the eluate was adjusted to 1.3 with 6 N HCl, and pepsin (2 μg) dissolved in 2 μL of aqueous HCl (pH 1.3) was added. The ratio of pepsin to NAT2 was approximately 1:100 (w/w). After incubation for 2 h at 25 °C, the peptides were separated by rpHPLC as described above and screened by MALDI-TOF MS. MALDI-TOF data were collected on a Bruker (Billerica, MA) Biflex III instrument, equipped with an N_2 laser (337 nm, pulse length of 3 ns) and a microchannel plate detector. Data were collected in reflectron mode, with positive polarity, with an accelerating potential of 19 kV. Samples were prepared by mixing (1:1) them with a methanol stock solution of α-cyano-4-hydroxycinnamic acid (Hewlett-Packard), which was diluted 1:1 with 50% acetonitrile and 0.01% trifluoroacetic acid before being used. Fractions containing peptides of interest were directly infused into the ESI-MS instrument as described above. A tandem mass spectrum was obtained for a doubly charged species with a molecular mass of 1104 Da with the sequence DQIVRKKG-GWCLQVNHL by using a 30% collision energy and a 3 Da mass tolerance.

RESULTS

Kinetics of Inactivation of NAT2 by Thiol Specific Modifiers. IAA and IAM are two thiol specific modifiers commonly used to probe the reactivity of cysteine residues in proteins. The reactive sulfhydryl group must, however, be sufficiently nucleophilic to react rapidly in solution. NAT2 exhibited a pseudo-first-order, concentration-dependent, and time-dependent loss of activity when incubated with IAM or BAM (see the Supporting Information). The reaction of NAT2 with IAM and BAM is markedly faster than with either IAA or BAA. NAT2 retained more than 60% of its original activity after incubation with either 2 mM IAA or 3 mM BAA for 60 min. The reaction of IAM with NAT2 was also independent of ionic strength, as addition of nearly 0.98 M NaCl did not affect the rate of inactivation (see the Supporting Information).

The second-order rate constants (k_{inact}) for the NAT2 reaction with BAM and IAM are 426.9 ± 21.0 and 802.7 ± 4.0 M^{-1} s^{-1}, respectively (Table 1). The 2-fold difference in the reactivity of the inhibitors is expected and consistent with the electronic properties of the leaving groups (Br or I) (*24*). The k_{inact} of 802.7 ± 4.0 M^{-1} s^{-1} is comparable with the maximum k_{inact} of either IAM or IAA with papain (Table

Table 1: Comparison of Inactivation Rate Constants (k_{inact}) of Cysteine Specific Affinity Labels for NAT2 and Papain

	k_{inact} (M^{-1} s^{-1})		
	NAT2	papain[a]	
	pH 7.0	pH 6.0	pH 10.0
iodoacetic acid	not determined[b]	1100	20
bromoacetic acid	not determined[c]	–	–
iodoacetamide	802.7 ± 4.0	14.5	976
bromoacetamide	426.9 ± 21.0	–	–

[a] Data from ref *35*. [b] More than 60% of the original activity remained after a 60 min incubation with 2 mM iodoacetic acid. [c] More than 60% of the original activity remained after a 60 min incubation with 3 mM bromoacetic acid.

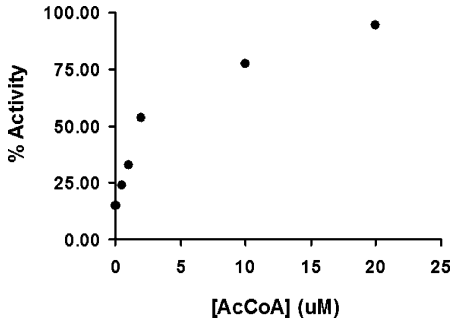

FIGURE 2: Effect of AcCoA on NAT2 inactivation by iodoacetamide. Inactivation reactions were conducted at pH 7.0 and 37 °C with 2 μM iodoacetamide. The results represent the means of two experiments, each of which was carried out in triplicate.

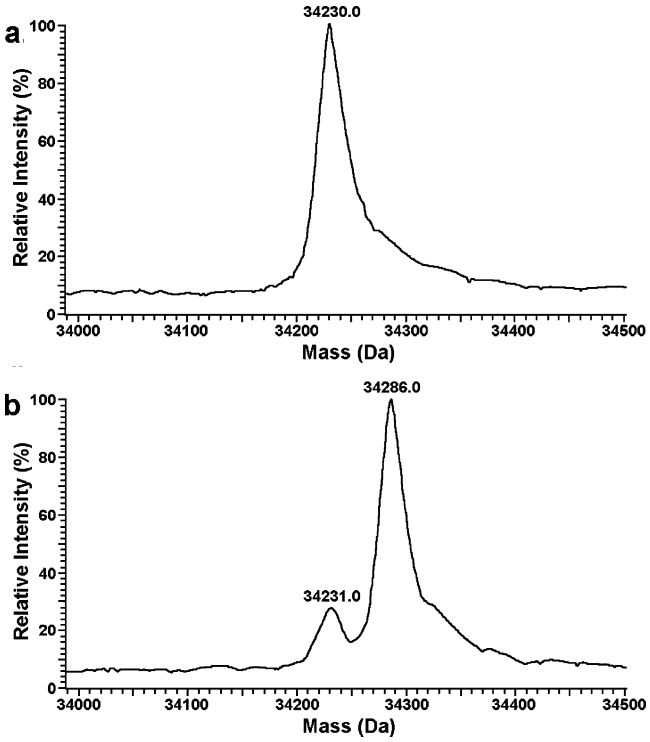

FIGURE 3: Deconvoluted ESI mass spectrum of NAT2 with (b) and without (a) the addition of iodoacetamide (120 μM) at 25 °C.

1), thus indicating the involvement of a highly reactive thiolate nucleophile in both NAT2 and papain. The reaction order for BAM and IAM (1.2 and 1.1, respectively) suggests that inactivation follows a 1:1 stoichiometric relationship and that a single modification is associated with each inactivation event. Furthermore, incubation of NAT2 with AcCoA prevents inactivation by IAM in a concentration-dependent manner, providing additional evidence that the site of alkylation is within the active site of the enzyme (Figure 2).

Identification of the Reactive Residue in NAT2. To verify that a single modified site is present on NAT2 that had been treated with IAM, ESI-MS of the protein was obtained with and without the addition of the inhibitor (Figure 3). A molecular mass of 34 230 Da was obtained for the native (untreated) protein, in agreement with the theoretical mass of 34 233 Da.[2] Incubation of the enzyme with a 2:1 molar ratio of IAM to NAT2 for 5 min at 25 °C results in two prominent peaks in the mass spectrum. The first peak corresponded to the native protein, while the larger second peak of 34 286 Da was consistent with the native protein with a single covalent addition of an acetamido group (theoretical addition of 57 Da).

To identify the specific amino acid residue in NAT2 that was modified by IAM, the alkylated NAT2 was digested with pepsin. The peptides were fractionated by rpHPLC. The composition of each fraction was screened by MALDI-TOF mass spectrometry. A modified peptide with a monoisotopic mass of 2207.0 Da was identified, which corresponded to the peptide sequence DQIVRKKRGGW<u>C</u>LQVNHL[3] (Asp-57−Leu-74), with a theoretical mass of 2207.2 Da. No other peak was found in the MALDI-TOF spectra of any fraction that was consistent with another modified residue. The rpHPLC fraction containing the peptide with a mass of 2207.0 Da was infused directly into an ESI-MS instrument. A doubly charged peak [$(M + 2H)^{2+}$] with a monoisotopic mass of 1104.0 Da was found, and the daughter MS/MS spectrum was collected (Figure 4). Most of the b and y ions were identified and closely matched the theoretical ions (see the Supporting Information and Table 1). The b_{11} ion (1324.6 m/z), the $b_{13}-NH_3$ ion (1580.6 m/z), and the y_6 ion (723.3 m/z) unambiguously identified the active site Cys-68 as the carbamidomethylated residue.

Effect of pH and D_2O on Iodoacetamide Inactivation of NAT2. Results of the inactivation of NAT2 with IAM suggest that the active site Cys-68 is highly reactive. Presumably, the thiolate of Cys-68 acts as the nucleophile in this reaction, implying a significant shift in the pK_a of the thiol group. To determine the pK_a of Cys-68, the pH dependence of inactivation by IAM was evaluated (Figure 5). The observed k_{inact} was determined over a pH range of 5.0−9.0. In this pH range, the control activity (activity in the absence of IAM) remained constant. Below pH 5.0, the enzyme control activity was greatly reduced. For example, at pH 4.5, less than 30% of the control activity was recovered, possibly due to protein instability.

The k_{inact} for NAT2 inactivation with IAM increased as a function of pH to a maximum at pH 6.4, and then decreased slightly until a plateau, 63% of the maximum k_{inact}, was reached above pH 8.0. The pH profile indicates NAT2 has two ionization states (E and EH) that can both undergo the alkylation reaction with IAM (Scheme 2A). The acid limb

[2] The theoretical mass includes four additional residues (Gly, Thr, Leu, and Glu) at the N-terminus of NAT2 from cleavage of the fusion protein.

[3] <u>C</u> is the active site cysteine (Cys-68) modified by carbamidomethylation.

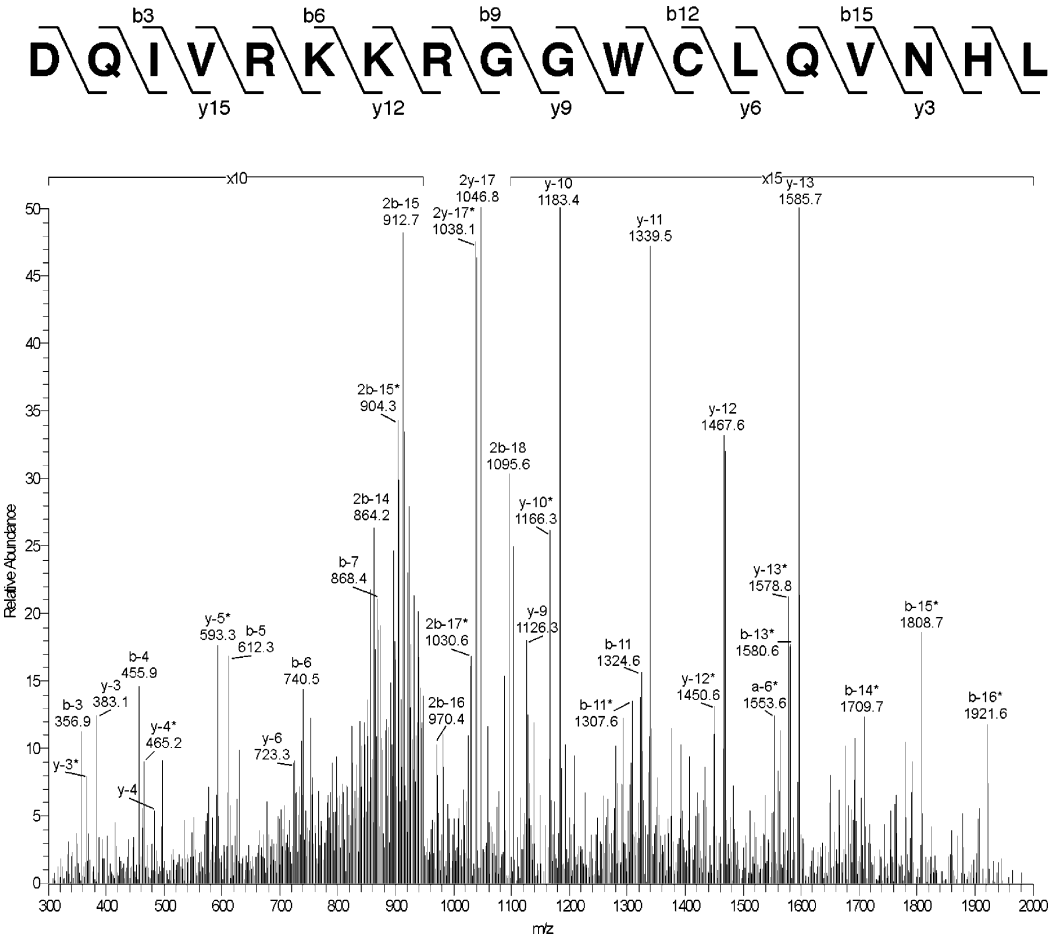

FIGURE 4: ESI tandem mass spectrum of pepsin-digested peptide (Asp-57−Leu-74 in the NAT2 sequence) DQIVRKKRGGWCLQVNHL. The active site Cys-68 was modified by iodoacetamide. 2b(y)-n indicates a doubly charged species, and an asterisk denotes an ion minus NH_3.

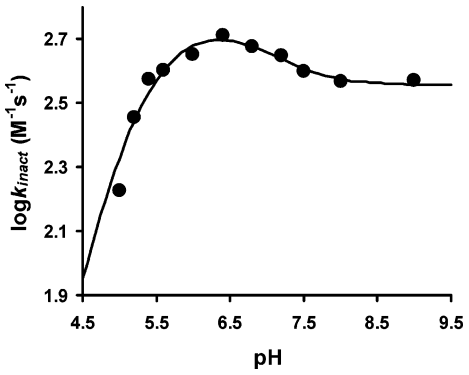

FIGURE 5: pH dependence of NAT2 inactivation by iodoacetamide. Experimental conditions are described in Experimental Procedures. The line was fit to the experimental data according to eq 4a, and the best fit parameters were as follows: $pK_{a1} = 5.23 \pm 0.09$ and $pK_{a2} = 6.95 \pm 0.27$.

exhibited one log unit of change in the value of k_{inact} over a single pH unit, consistent with the titration of a single ionizable group in the inactivation reaction. Fitting of the pH data to eq 4a yielded $(k_{inact})_{lim}$ at 571.43 ± 31.75 M^{-1} s^{-1}, a ratio (r) of k_{inact} values at two ionization states (E vs EH) of 0.63, an apparent pK_{a1} of 5.23 ± 0.09, and an apparent pK_{a2} of 6.95 ± 0.27.

Solvent kinetic isotope effects on iodoacetamide inactivation were determined by measuring inactivation rate constants in both H_2O and 95% D_2O at two different pLs, 6.4 and 9.0 (Figure 6). The inactivation occurred at a faster rate in D_2O than in H_2O at both pLs. In 95% D_2O, $k^H_{inact}/k^D_{inact} = 0.65 \pm 0.02$ at pL 6.4 and 0.61 ± 0.06 at pL 9.0. Because of its unusual inverse fractionation factor ($\Phi = 0.4-0.5$) (*23*), at first glance, the inverse SKIE could be assigned to the active site cysteine thiol group (*25*−*28*). However, the pK_{a1} value of 5.23 is likely to depend on contributions of both side chains of the thiolate−imidazolium ion pair (Cys-SH−His-ImH^+, Scheme 4). As the pH increases, the Cys-SH−His-ImH^+ pair will be deprotonated to form either a neutral pair (Cys-SH−His-Im) or an ionic pair (Cys-S^-−His-ImH^+). Consequently, the equilibrium between these tautomeric forms of the thiolate−imidazolium pair would furnish the necessary inverse isotopic effect, if the ionic pair is the only reactive form of NAT2 (*29*, *30*).

Single-Turnover Kinetic Analysis for NATs. A ping-pong kinetic mechanism predicts that an acetyl-enzyme intermediate is formed in the reaction of NAT2 and AcCoA, and that the acetyl group is subsequently transferred to the arylamine in the second half-reaction. If enzyme deacetylation by solvent is slow relative to acetylation, single-turnover kinetics should allow the formation of the acetyl-enzyme intermediate to be monitored. By using excess PNPA (80−1500 μM) as an acetyl donor, the rate of formation of the acetyl-enzyme intermediate in the first half-reaction was determined by single-turnover experiments with stopped flow techniques. The progress curves, recorded by the increase in absorbance at 400 nm due to formation of *p*-nitrophenol, displayed substrate concentration-dependent burst kinetics (Figure 7a).

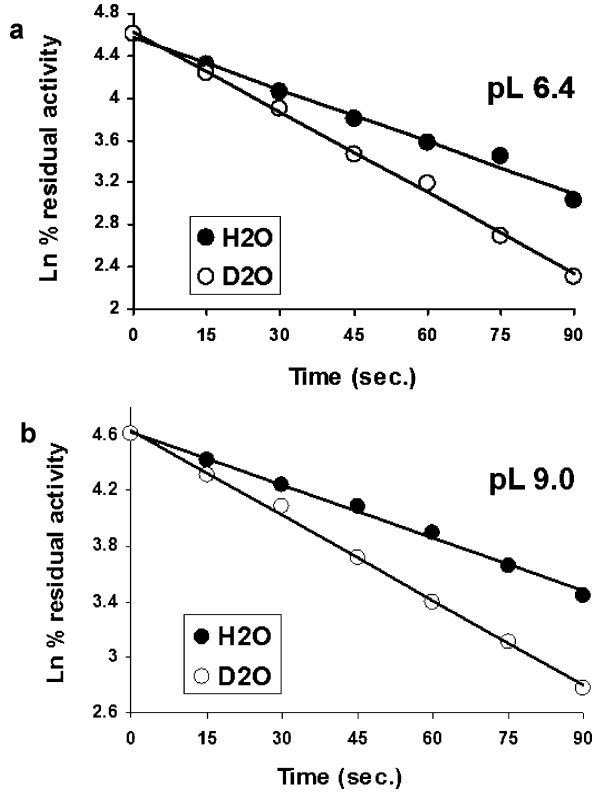

FIGURE 6: Solvent kinetic isotope effects for iodoacetamide inactivation at pL 6.4 (a) and pL 9.0 (b). Experiments were performed as described in Experimental Procedures. The values of k_{inact} were obtained by fitting the data to eq 2. (a) $k^{H}_{inact} = 662 \pm 14.14$ M^{-1} s^{-1}, and $k^{D}_{inact} = 1024 \pm 22.63$ M^{-1} s^{-1}. (b) $k^{H}_{inact} = 508 \pm 35.59$ M^{-1} s^{-1}, and $k^{D}_{inact} = 830 \pm 25.45$ M^{-1} s^{-1}.

Since only one exponential decay curve was observed and no acetyl-enzyme hydrolysis could be detected during the 100 ms time period of these experiments, the data were fit to a single exponential and the rates were extracted. The amplitude was found to be independent of PNPA concentration and equal to 0.94 ± 0.02 enzyme equivalent. We attempted to determine a K_m^{acetyl} for PNPA, but were unable to observe saturation within the substrate concentration range (80−1500 μM). Figure 7b is a plot of the substrate concentration versus the observed first-order rate constant (k_{obs}). It indicates $K_m^{acetyl} \gg$ [PNPA] (eq 7). The slope of the line in Figure 7b represents a second-order rate constant k_2/K_m^{acetyl} of $(1.4 \pm 0.05) \times 10^5$ M^{-1} s^{-1} (eq 8), which is more than 100 times faster than the inactivation rate constant (k_{inact}) observed for IAM. The values of K_m^{acetyl} and k_2 were estimated to be 9 ± 5.7 mM and 1301 ± 716 s^{-1}, respectively. If k_{-1} is assumed to be diffusion-limited, then $k_{-1} \gg k_2$ and $K_m^{acetyl} \approx K_S$, suggesting that PNPA is a low-affinity substrate for NAT2.

Steady State Kinetics of Acetyl-Enzyme Hydrolysis. Single-turnover kinetics demonstrated that NAT2 acetylation was characterized by rapid enzyme acetylation, followed by rate-limiting deacetylation (k_3, eq 12). To measure the rate of acetyl-enzyme hydrolysis (k_3), NAT2 was incubated with 320 μM PNPA and the absorbance recorded at 400 nm continuously for 12 min (Figure 8). After the initial burst, the formation of *p*-nitrophenol proceeded linearly. The rates of hydrolysis at enzyme concentrations of 4 and 8 μM were found to be 31.2 ± 0.5 and 67.1 ± 0.45 nM/s, respectively. Since the second-order rate constant of acetylation (k_2/K_m^{acetyl}) is 1.4×10^5 M^{-1} s^{-1}, the k_{obs} for enzyme acetylation at a substrate concentration of 320 μM was calculated to be 44.8 s^{-1}. Consequently, the rate of acetyl-enzyme hydrolysis (k_3) is equal to $(7.85 \pm 0.65) \times 10^{-3}$ s^{-1}, which corresponds to an acetyl-enzyme half-life ($t_{1/2}$, eq 13) of 88.3 ± 8.3 s. The stability of the acetyl-enzyme intermediate may be enzyme-

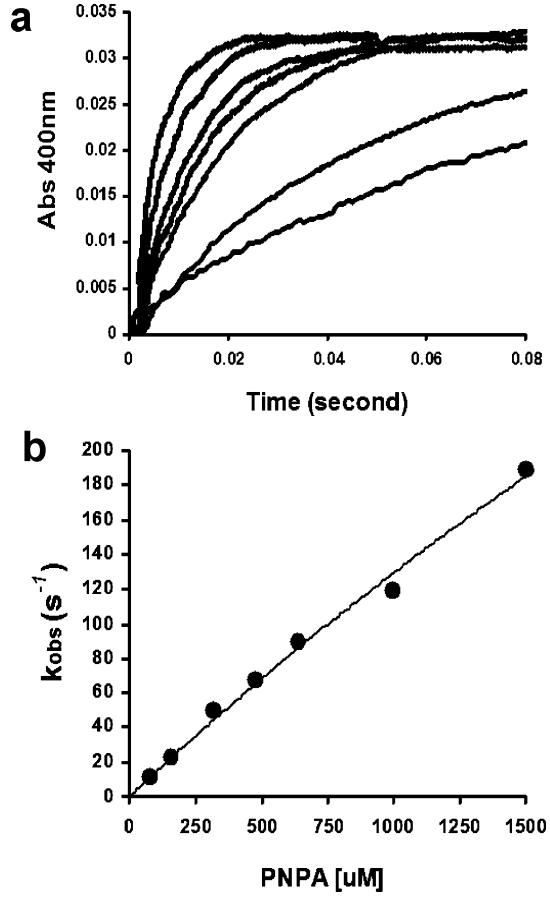

FIGURE 7: Pre-steady state kinetics of formation of the acetyl-enzyme intermediate. (a) Single-turnover time course of formation of *p*-nitrophenol. The experimental data are fit to eq 5 at PNPA concentrations of 80, 160, 320, 480, 640, 1000, and 1500 μM (from bottom to top). (b) Plot of the determined rate constants as a function of the PNPA concentration. The data were fit to eq 8, which gave a k_{cat}/K_m^{acetyl} of $(1.4 \pm 0.05) \times 10^5$ M^{-1} s^{-1}.

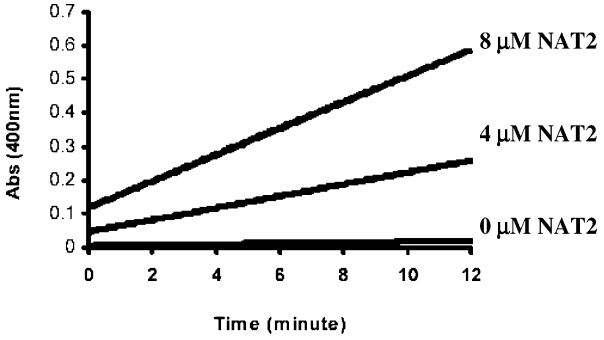

FIGURE 8: Steady state rate of NAT2-catalyzed PNPA hydrolysis. The PNPA concentration was 320 μM, and the NAT2 concentration was 0, 4, or 8 μM. Reactions were performed in duplicate at pH 7.0 and 25 °C as described in Experimental Procedures. The rate of nonenzymatic hydrolysis (0 μM NAT2), 1.95 ± 0.0 nM/s, was subtracted from that of enzymatic reactions, which gave values of 31.2 ± 0.5 nM/s for 4 μM NAT2 and 67.1 ± 0.45 nM/s for 8 μM NAT2. Data were fit to eq 12 which gave a k_3 of $(7.85 \pm 0.65) \times 10^{-3}$ s^{-1}.

Scheme 4

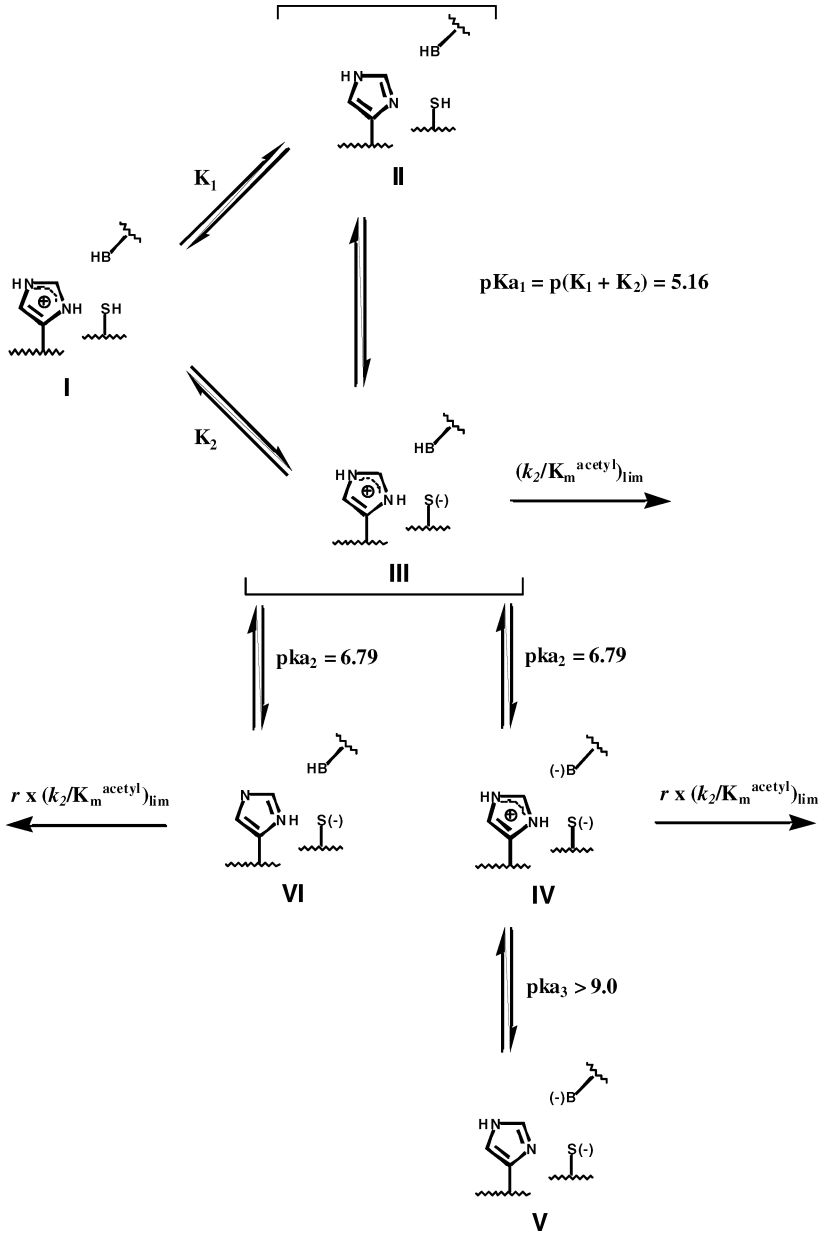

dependent, since a half-life of <1 min was observed for the pigeon NAT (*31*).

Effect of pH and D_2O on Single-Turnover Kinetics. The ability of NAT2 to be rapidly acetylated by PNPA and alkylated by IAM suggests that the active site cysteine thiolate is highly nucleophilic. In addition, the pK_{a1} of 5.23 ± 0.09 is consistent with a mechanism relying on a preformed active site thiolate−imidazolium ion and not general base catalysis. Therefore, the pH dependence of enzyme acetylation under single-turnover conditions with 320 μM PNPA was determined for NAT2 over a pH range from 5.0 to 9.0. Since the K_m^{acetyl} is at least 10 times greater than the substrate concentration, the observed rate constant (k_{obs}) for a single turnover equals (k_2/K_m^{acetyl})[PNPA]$_0$ (eq 8). Values of k_2/K_m^{acetyl} were plotted as a function of pH (Figure 9). From the plot, the values of 5.16 ± 0.04 and 6.79 ± 0.25 were calculated for pK_{a1} and pK_{a2}, respectively (eq 4b). A value of (1.6 ± 0.02) × 10^5 M^{-1} s^{-1} for $(k_2/K_m^{acetyl})_{lim}$ was observed, and the ratio, r, of the values for k_2/K_m^{acetyl} for the two ionization states, E and EH, was found to be 0.76 ± 0.02. These results are consistent with the pH dependence studies of NAT2 inactivation by IAM, yielding nearly identical pK_a values. The pL dependence of SKIE on enzyme acetylation was examined over the pL range of 5.0−9.0 with a reaction buffer composed of 95% D_2O. From the pL versus rate plot, values of 5.26 ± 0.07 and 6.59 ± 0.16 were calculated for pK_{a1} and pK_{a2}, respectively, in deuterated buffer. In contrast to the results observed in nondeuterated buffer, NAT acetylation was not observed below a pD of 5.6. The ratio of k_2/K_m^{acetyl} in H_2O versus D_2O across the pH plot corresponded to an inverse solvent isotope effect of 0.6 ± 0.03 at pL 6.4 and 0.65 ± 0.02 at pL 9.0.

To assess the protonation state of the reactive side chains along the reaction coordinate for NAT2 acetylation, a proton inventory analysis was carried out by determining the effect of variable D_2O buffer composition on k_2/K_m^{acetyl} (Figure 10). The linear plots under both pL conditions indicate that deprotonation of the thiolate−imidazolium ion does not occur in the transition state. A linear relationship of k_0/k_n with the mole fraction of D_2O (n) was observed with a negative slope

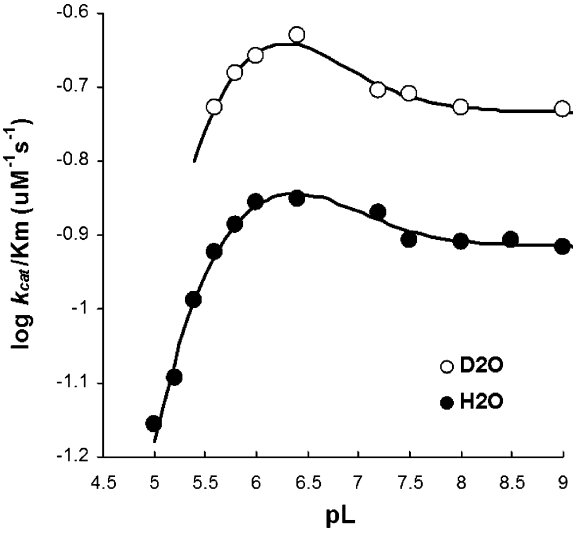

FIGURE 9: pL dependence of the NAT2 single-turnover kinetic reaction with PNPA in H_2O (●) and D_2O (○). Experiments were performed as described in Experimental Procedures. The curves were drawn through the experimental points by fitting to eq 4b. The calculated pK_a values in H_2O were 5.16 ± 0.04 and 6.79 ± 0.25, whereas those in D_2O were 5.26 ± 0.07 and 6.59 ± 0.16.

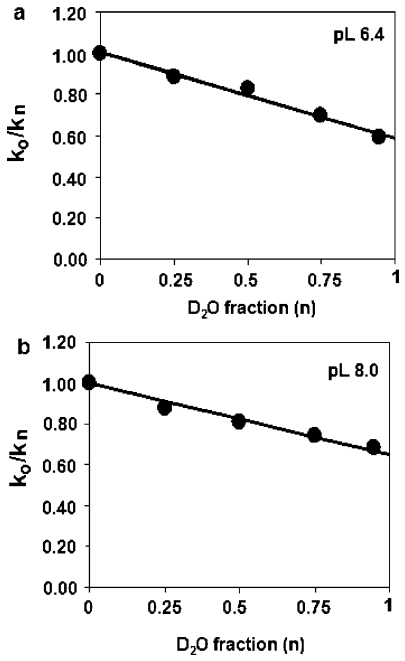

FIGURE 10: Proton inventory studies of NAT2 single turnover with PNPA at pL 6.4 (a) and 8.0 (b). Experiments were performed as described in Experimental Procedures. Pseudo-first-order rate constants (k_{obs}) were obtained by fitting the data to eq 5. k_o represents the k_{obs} in 0 mole fraction D_2O, and k_n represents the k_{obs} in n mole fraction D_2O. The experimental data were fit to a line with an R^2 of 0.99 (a) or 0.98 (b). According to eq 14, the reactant state fractionation factor (Φ) was determined to be 0.58 at pL 6.4 and 0.65 at pL 8.0.

of 0.42 for pL 6.4 (Figure 10a). The solvent isotope effect was extrapolated to 0.58 (pL 6.4) in 100% D_2O. At pL 8.0, a similar linear plot was observed with a negative slope of 0.35, corresponding to the solvent isotope effect of 0.65 at 100% D_2O (Figure 10b). Thus, a similar reaction mechanism is employed by the enzyme under both basic and acidic conditions.

Site-Directed Mutagenesis of D122N and D122A. According to SDS−PAGE and quantitative Western blot analysis of cell lysates, the overexpression level of wild-type, D122N, and D122A NAT2 is similar (data not shown). However, the mutant enzymes were found only in the insoluble fraction of the cell lysate. No activity was observed in the soluble fraction for either mutant. The refolded and soluble mutant protein was found to be devoid of transacetylase activity. In contrast, at least 25−50% of the fusion protein activity could be recovered from insoluble wild-type NAT2 after refolding under identical conditions (data not shown).

DISCUSSION

Arylamine *N*-acetyltransferases constitute a ubiquitous enzyme class that has been shown to be important for drug metabolism and the bioactivation of carcinogenic arylamines. NATs catalyze the AcCoA-dependent acetylation of a variety of arylamines (*1*, *3*, *8*). NATs employ a bi-bi ping-pong mechanism in which an active site cysteine is first acetylated, followed by the transfer of the acetyl group to an arylamine. Recently, X-ray structural studies of the *S. typhimurium* NAT revealed that activation of the active site cysteine may be facilitated by a proximal histidine and aspartic acid, thus forming a putative catalytic triad (*8*). It was suggested that this arrangement of catalytic functional groups is reminiscent of cysteine proteases, such as papain (*8*). Sequence analysis studies have demonstrated that the residues of the triad are strictly conserved across all known prokaryote and eukaryote NATs. Model building studies based on the bacterial structure have also suggested that the general structural features of the catalytic domain and positions of the side chains of the triads for bacterial and mammalian NATs are likely to be highly similar (*10*, *11*). However, except for studies of the reaction order and deletion mutagenesis experiments with the bacterial enzyme, little is known about the catalytic mechanism for NATs (*32*−*34*). Since the sequences of mammalian NATs are >60% identical, and the hamster enzyme is the only eukaryote NAT that can presently be readily overexpressed and purified to homogeneity, we have chosen to begin examining the catalytic mechanism of mammalian NAT catalysis with amino acid modification, kinetic, SKIE, and site-directed mutagenesis experiments.

Active Site Environment and Reactivity. The alkylating agents IAA and IAM have been used successfully to investigate the chemical properties of active site cysteine-containing enzymes, such as papain (*15*, *35*), chalcone synthase (*36*), and protein tyrosine phosphatases (*26*, *37*). In general, at neutral pH, IAM reacts approximately 10-fold faster with sulfur nucleophiles than IAA (*35*). Nevertheless, the rate of inactivation of papain by IAA has been shown to be at least 15-fold higher than by IAM at neutral pH, while at high pH, IAM is able to inactivate the enzyme at a faster rate than IAA (Table 1) (*35*). The enhanced reactivity of IAA at neutral pH was explained by the electrostatic interactions of the carboxylate of IAA with a solvent accessible histidine imidazolium (*35*, *37*). In contrast, an ion pair interaction between the triad histidine of NAT2 and the alkylation reagents is unlikely, since the rate of alkylation by IAM or BAM was at least 800- or 400-fold greater than the rate of alkylation by IAA or BAA, respectively.

The approximately 2-fold difference in the rate of NAT2 inactivation by IAM and BAM is similar to that observed for the reaction of glutathione with IAM and BAM, indicat-

ing that the active site is able to fully accommodate either halide (*24*). In addition, as expected from the relative order of reactivity of IAM and BAM, in both cases, a slope of unity was observed, thus indicating that alkylation of one reactive group is necessary for inactivation of the enzyme. The identity of the active site reactive nucleophile as Cys-68 was initially inferred by demonstrating that preincubation of NAT2 with AcCoA could effectively block enzyme inactivation by IAM. Mass spectral analysis of IAM-inactivated NAT2 confirmed this conclusion by identifying Cys-68 as the only site of NAT2 alkylation.

In contrast to the case with papain, the ability of both IAM and BAM, but not IAA and BAA, to efficiently alkylate NAT2, and the independence of the rate of IAM alkylation on ionic strength, indicate a relatively nonpolar active site in which the catalytic triad histidine is inaccessible to the carboxylate of IAA. This conclusion is supported by modeling studies of mammalian NATs based on the X-ray structure of the bacterial enzyme (*10*, *38*). Consequently, like that of bacterial NATs, the active site of mammalian NATs is likely characterized by a deep hydrophobic pocket in which the accessibility of the histidine to solvent has been restricted (*10*, *11*). The results reported by Andres on the alkylation of rapid acetylator rabbit NAT provide further evidence of a nonpolar, hydrophobic active site (*33*). IAA (5 mM) caused 30−40% inactivation of rabbit NAT in 5 min, and a 30 min incubation was required for the complete loss of activity. Bromoacetanilide, which is an un-ionized, lipophilic alkylating agent, was a significantly more effective inactivator, causing complete and irreversible inhibition within 30 s at 25 °C (*33*). Similarly, we have found that lipophilic nonpolar reagents are highly effective, active site-directed, alkylating agents for NATs (*39*).

Having established that the catalytically essential Cys-68 was the site of alkylation by IAM, we determined the effect of varying pH on the rate of alkylation. As can be seen from Figure 5, the rate of alkylation was attenuated only under acidic conditions. Typically, for enzymes that require nucleophilic attack by a cysteine thiol, such as cysteine proteases, the pK_a for the active site cysteine lies in the range of 3.3−5.5, which is 3.0−5.0 pK_a units lower than the pK_a normally observed for a cysteine thiol group. This has been interpreted as evidence for the direct interaction of the histidine imidazole with the cysteine thiol group, resulting in formation of a thiolate−imidazolium ion at neutral pH (*15*). Homology modeling, based on the crystal structure of bacterial NAT, has suggested that the spatial arrangement of the active site side chains is maintained for human as well as other mammalian NATs (*10*, *11*). Therefore, our observation of a pK_a of 5.23 ± 0.03 for Cys-68 is consistent with an interaction with an imidazole, presumably His-107. This conclusion was supported by the finding of an inverse SKIE on NAT2 inactivation by IAM, signifying that the thiolate is largely deprotonated before inactivation.

The maximal rate of 802 M^{-1} s^{-1} observed for inactivation of NAT2 with IAM is very similar to the value of 976 M^{-1} s^{-1} observed for papain, but unlike papain, for which the maximal rate of inactivation by IAM is only realized at pH ≥9, the maximal value for NAT2 is observed over a pH range of 6.0−9.0. Indeed, the rate of inactivation of papain by IAM is approximately 70-fold greater at pH 9.0 than at pH 6.0. The increase in the rate of inactivation at higher pH was believed to be due to the deprotonation of histidine imidazolium, which leads to the free thiolate anion, instead of the thiolate−imidazolium ion pair, acting as the reactive species. The pK_a data for NAT2 can be interpreted in terms of a pK_a (>9.5) for the active site histidine substantially greater than that observed for cysteine proteases (pK_a ≈ 8−9). This seems plausible given the position of His-107 between the thiolate of Cys-68 and, as observed for the bacterial enzyme, a solvent inaccessible Asp-122 carboxylate. Therefore, pK_{a2} is likely the result of a pH-dependent conformation change rather than deprotonation of the His-107 imidazolium in NAT2. This is further supported by the similar inverse isotope effect observed at pL 6.4 as well as pL 9.0, indicating that the thiolate−imidazolium ion pair is the reactive species even at high pH.

Enzyme Acetylation. Although the active site inactivation experiments provide insights into the reactivity of the active site, they do not necessarily address the significance of these characteristics to enzyme catalysis. Our finding that PNPA was a substrate for hamster NAT2 allowed us to directly compare enzyme acetylation and alkylation. Since the rate of enzyme deacetylation was shown to be several orders of magnitude lower than that of acetylation, the transient state kinetic curve was best fit by a single-exponential curve (Figure 7a) with an amplitude corresponding to the acetylation of nearly 1 equiv of enzyme. As in the alkylation experiments, enzyme acetylation with PNPA is fast and nonsaturable, with a second-order rate constant (k_2/K_m^{acetyl}) 100-fold greater than the second-order rate constant for IAM inactivation. Subsequent steady state analysis revealed that the rate of enzyme acetylation was at least 24000-fold greater than the rate of enzyme deacetylation; thus, $k_2 \gg k_3$, and $k_{cat} \approx k_3$. To account for the facilitation of arylamine acetylation in an aqueous environment, this conclusion seems to be reasonable, if not a necessity. Consequently, the active site functions not only to accelerate enzyme acetylation but also to reduce the rate of thioester hydrolysis.

Examination of the pH versus rate profile indicates that catalysis is governed by the pK_a values of 5.16 ± 0.04 and 6.79 ± 0.25, which are nearly identical to the values obtained from IAM inactivation. The pH versus rate profile, therefore, is entirely dependent on the reactivity of the active site thiolate−imidazolium ion pair. An apparent pK_a of 5.2 is generally assigned to the catalytic cysteine (*26*, *36*, *37*). However, Menard and Storer have proposed a more complicated model for thiolate−imidazolium facilitated catalysis in which the apparent pK_a represents an overall pK_a of both the imidazolium and cysteine sulfhydryl; i.e., pK_a = p(K_1 + K_2) (Scheme 4) (*40*). On the basis of the apparent pK_a values for the wild type, and the Asn-175 to Gln or Ala mutant, the intrinsic pK_a values for the cysteine sulfhydryl and the histidine imidazolium of papain were approximately 4.43 and 5.08, respectively (*40*). In our case, however, the intrinsic pK_a values for NAT2 were not able to be determined, since neither the Asn-122 mutant nor the Ala-122 mutant was active.

Two explanations could be envisioned to justify the similar inverse isotope effect and proton inventory results under both neutral and basic conditions (pH 8.0) (Scheme 4). First, a pH-dependent protein conformational change that modestly reduces the rate of acetylation could be responsible for the second pK_a value of 6.79. Further deprotonation of the

Scheme 5: Proposed Mechanistic Options for NAT2 Acetylation by PNPA at Neutral pH

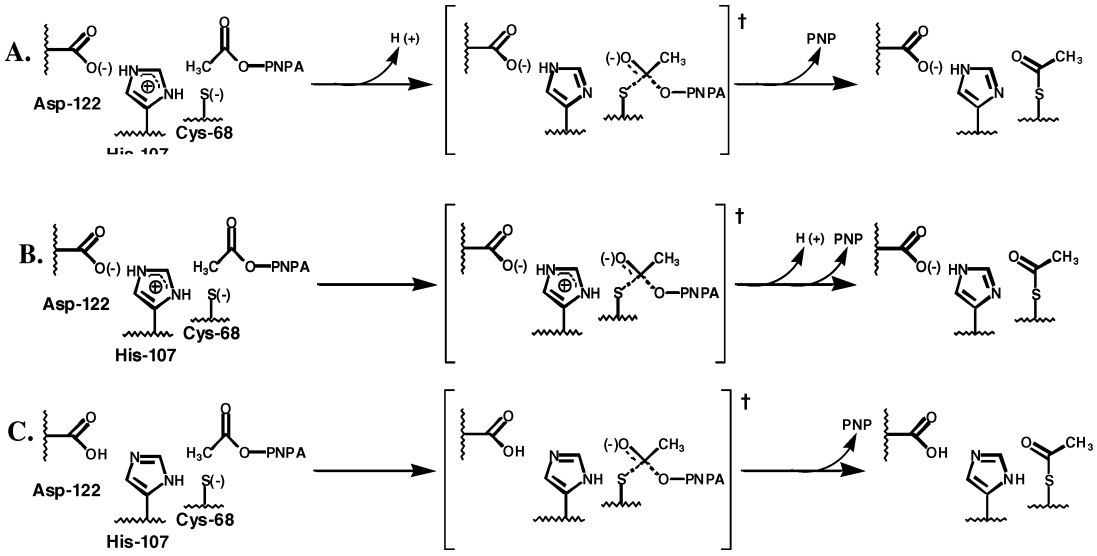

thiolate−imidazolium ion pair (IV) to the thiolate imidazole (V) would occur under only basic conditions (pK_a > 9.0). Consequently, at neutral pH, two pathways for NAT2 acetylation are possible (Scheme 5A,B) Although we are unable to determine from our experimental results whether deprotonation of the thiolate−imidazolium pair occurs in a step before or after formation of the transition state, on the basis of previous studies of enzyme-catalyzed acetyl transfer reactions with PNPA, the process likely proceeds through a concerted process and not by formation of a tetrahedral intermediate (*41*, *42*). An alternative explanation, based on deprotonation of the thiolate−imidazolium pair (III) to form the thiolate imidazole (VI), is also possible, but dependent on an active site preference for an imidazole tautomer capable of forming a strong hydrogen bond with the thiolate and Asp-122 (Scheme 5C). The inability of the Asp-122 to asparagine mutation to support catalysis and a pH−rate profile that reflects a decrease and not an increase in the rate of acetylation argues against this mechanistic proposal.

MECHANISTIC CONCLUSIONS

Although a structure of neither hamster nor other eukaryote NAT is available at present, and the sequences of bacterial and mammalian NATs are less than 30% identical, the alkylation results are consistent with the placement, as observed for the bacterial enzyme, of the Cys-His-Asp catalytic triad deep within the interior of the protein. Site-directed mutagenesis studies support this conclusion, since Asp-122 appears to be both structurally and catalytically essential.

Consistent with the alkylation experimental results, NAT2 kinetic and isotope effect experiments strongly support an enzyme acetylation mechanism that relies on a thiolate−imidazolium ion pair, but not general acid base catalysis. The pH dependence of the reaction appears to be governed by the pK_a of the thiolate−imidazolium pair and a probable protein conformational change (Scheme 4). Although Asp-122 could be responsible for the conformational change, it seems doubtful given the importance of this residue to catalysis and, based on homology modeling, its likely inaccessibility to solvent. Nevertheless, at physiological pH, acetylated NAT2 stands poised, with deprotonated His-107 in its proximity, to facilitate subsequent transacetylation by arylamine substrates (Scheme 5). Whether the stability of the acetylated enzyme is a function of the ability of the active site to facilitate nucleophilic attack by the incoming arylamine substrate at the expense of hydrolysis and/or solvent sequestration remains to be determined. Ongoing analysis of the acetyl transfer to appropriate arylamine substrates will address these fundamental NAT mechanistic questions.

ACKNOWLEDGMENT

We thank Dr. Thomas Krick and Dr. LeeAnn Higgins of the Mass Spectrometry Consortium for the Life Sciences at the University of Minnesota for expert assistance with ESI-MS and MALDI-TOF MS. We thank Dr. Issa S. Issac for assistance with the AcCoA protection and ionic strength experiments. We thank Dr. Brian Brazeau for assistance with the stopped flow instrument and Dr. Richard L. Schowen for his very helpful critical comments.

SUPPORTING INFORMATION AVAILABLE

Time- and concentration-dependent inactivation of NAT2 by IAM (Figure 1), effect of ionic strength on NAT2 inactivation by IAM (Figure 2), observed inactivation rate constant plotted as a function of BAM or IAM concentration (Figure 3), and identification of b and y ions obtained by MS/MS analysis (Table 1). This material is available free of charge via the Internet at http://pubs.acs.org.

REFERENCES

1. Hanna, P. E. (1994) *N*-Acetyltransferases, *O*-acetyltransferases, and *N*,*O*-acetyltransferases: enzymology and bioactivation, *Adv. Pharmacol. 27*, 401−430.
2. Hanna, P. E. (1996) Metabolic activation and detoxification of arylamines, *Curr. Med. Chem. 3*, 195−210.
3. Levy, G. N., and Weber, W. W. (2002) *Enzyme systems that metabolise drugs and other xenobiotics*, (Ioannides, C., Ed.) John Wiley & Sons, Ltd., New York, pp 441−457.
4. Hein, D. W., Doll, M. A., Fretland, A. J., Leff, M. A., Webb, S. J., Xiao, G. H., Devanaboyina, U. S., Nangju, N. A., and Feng, Y. (2000) Molecular genetics and epidemiology of the NAT1 and NAT2 acetylation polymorphisms, *Cancer Epidemiol. Biomarkers Prev. 9*, 29−42.

5. Cheon, H. G., Boteju, L. W., and Hanna, P. E. (1992) Affinity alkylation of hamster hepatic arylamine *N*-acetyltransferases: isolation of a modified cysteine residue, *Mol. Pharmacol. 42*, 82−93.
6. Dupret, J. M., and Grant, D. M. (1992) Site-directed mutagenesis of recombinant human arylamine *N*-acetyltransferase expressed in *Escherichia coli*. Evidence for direct involvement of Cys68 in the catalytic mechanism of polymorphic human NAT2, *J. Biol. Chem. 267*, 7381−7385.
7. Watanabe, M., Sofuni, T., and Nohmi, T. (1992) Involvement of Cys69 residue in the catalytic mechanism of *N*-hydroxyarylamine *O*-acetyltransferase of *Salmonella typhimurium*. Sequence similarity at the amino acid level suggests a common catalytic mechanism of acetyltransferase for *S. typhimurium* and higher organisms, *J. Biol. Chem. 267*, 8429−8436.
8. Sinclair, J. C., Sandy, J., Delgoda, R., Sim, E., and Noble, M. E. (2000) Structure of arylamine *N*-acetyltransferase reveals a catalytic triad, *Nat. Struct. Biol. 7*, 560−564.
9. Sandy, J., Mushtaq, A., Kawamura, A., Sinclair, J., Sim, E., and Noble, M. (2002) The structure of arylamine *N*-acetyltransferase from *Mycobacterium smegmatis*: an enzyme which inactivates the anti-tubercular drug, isoniazid, *J. Mol. Biol. 318*, 1071−1083.
10. Rodrigues-Lima, F., Delomenie, C., Goodfellow, G. H., Grant, D. M., and Dupret, J. M. (2001) Homology modelling and structural analysis of human arylamine *N*-acetyltransferase NAT1: evidence for the conservation of a cysteine protease catalytic domain and an active-site loop, *Biochem. J. 356*, 327−334.
11. Rodrigues-Lima, F., and Dupret, J. M. (2002) 3D model of human arylamine *N*-acetyltransferase 2: structural basis of the slow acetylator phenotype of the R64Q variant and analysis of the active-site loop, *Biochem. Biophys. Res. Commun. 291*, 116−123.
12. Upton, A., Johnson, N., Sandy, J., and Sim, E. (2001) Arylamine *N*-acetyltransferases: of mice, men and microorganisms, *Trends Pharmacol. Sci. 22*, 140−146.
13. Payton, M., Mushtaq, A., Yu, T. W., Wu, L. J., Sinclair, J., and Sim, E. (2001) Eubacterial arylamine *N*-acetyltransferases: identification and comparison of 18 members of the protein family with conserved active site cysteine, histidine and aspartate residues, *Microbiology 147*, 1137−1147.
14. Polgar, L. (1973) On the mode of activation of the catalytically essential sulfhydryl group of papain, *Eur. J. Biochem. 33*, 104−109.
15. Polgar, L. (1974) Mercaptide-imidazolium ion-pair: the reactive nucleophile in papain catalysis, *FEBS Lett. 47*, 15−18.
16. Storer, A. C., and Menard, R. (1994) Catalytic mechanism in papain family of cysteine peptidases, *Methods Enzymol. 244*, 486−500.
17. Lewis, S. D., Johnson, F. A., and Shafer, J. A. (1981) Effect of cysteine-25 on the ionization of histidine-159 in papain as determined by proton nuclear magnetic resonance spectroscopy. Evidence for a His-159−Cys-25 ion pair and its possible role in catalysis, *Biochemistry 20*, 48−51.
18. Lewis, S. D., Johnson, F. A., and Shafer, J. A. (1976) Potentiometric determination of ionizations at the active site of papain, *Biochemistry 15*, 5009−5017.
19. Sticha, K. R. K., Sieg, C. A., Bergstrom, C. P., Hanna, P. E., and Wagner, C. R. (1997) Overexpression and large-scale purification of recombinant hamster polymorphic arylamine *N*-acetyltransferase as a dihydrofolate reductase fusion protein, *Protein Expression Purif. 10*, 147−153.
20. Bradford, M. M. (1976) A rapid and sensitive method for the quantitation of microgram quantities of protein utilizing the principle of protein-dye binding, *Anal. Biochem. 72*, 248−254.
21. Bergstrom, C. P., Wagner, C. R., Ann, D. K., and Hanna, P. E. (1995) Hamster monomorphic arylamine *N*-acetyltransferase: expression in *Escherichia coli* and purification, *Protein Expression Purif. 6*, 45−55.
22. Ward, A., Summers, M. J., and Sim, E. (1995) Purification of recombinant human *N*-acetyltransferase type 1 (NAT1) expressed in *E. coli* and characterization of its potential role in folate metabolism, *Biochem. Pharmacol. 49*, 1759−1767.
23. Schowen, K. B., and Schowen, R. L. (1982) Solvent isotope effects of enzyme systems, *Methods Enzymol. 87*, 551−606.
24. Dahl, K. H., and McKinley-McKee, J. S. (1981) The reactivity of affinity labels: a kinetic study of the reaction of alkyl halides with thiolate anions: a model reaction for protein alkylation, *Bioorg. Chem. 10*, 329−341.
25. Tipton, P. A., and Cleland, W. W. (1988) Carbon-13 and deuterium isotope effects on the catalytic reactions of biotin carboxylase, *Biochemistry 27*, 4325−4331.
26. Rudolph, J. (2002) Catalytic mechanism of Cdc25, *Biochemistry 41*, 14613−14623.
27. Quinn, D. M., and Sutton, L. D. (1991) *Enzyme Mechanism from Isotope Effects*, CRC Press, Boston.
28. Cleland, W. W. (1987) The use of isotope effects in the detailed analysis of catalytic mechanisms of enzymes, *Bioorg. Chem. 15*, 283−302.
29. Creighton, D. J., and Schamp, D. J. (1980) Solvent isotope effects on tautomerization equilibria of papain and model thiolamines, *FEBS Lett. 110*, 313−318.
30. Wandinger, A., and Creighton, D. J. (1980) Solvent isotope effects on the rates of alkylation of thiolamine models of papain. *FEBS Lett. 116*, 116−121.
31. Jencks, W. P., Gresser, M., Valenzuela, M. S., and Huneeus, F. C. (1972) Acetyl coenzyme A: arylamine acetyltransferase, *J. Biol. Chem. 247*, 3756−3760.
32. Andres, H. H., Kolb, H. J., Schreiber, R. J., and Weiss, L. (1983) Characterization of the active site, substrate specificity and kinetic properties of acetyl-CoA:arylamine *N*-acetyltransferase from pigeon liver, *Biochim. Biophys. Acta 746*, 193−201.
33. Andres, H. H., Klem, A. J., Schopfer, L. M., Harrison, J. K., and Weber, W. W. (1988) On the active site of liver acetyl-CoA. Arylamine *N*-acetyltransferase from rapid acetylator rabbits (III/J), *J. Biol. Chem. 263*, 7521−7527.
34. Riddle, B., and Jencks, W. P. (1971) Acetyl-coenzyme A: arylamine *N*-acetyltransferase. Role of the acetyl-enzyme intermediate and the effects of substituents on the rate, *J. Biol. Chem. 246*, 3250−3258.
35. Halasz, P., and Polgar, L. (1977) Negatively charged reactants as probes in the study of the essential mercaptide-imidazolium ion-pair of thiolenzymes, *Eur. J. Biochem. 79*, 491−494.
36. Jez, J. M., and Noel, J. P. (2000) Mechanism of chalcone synthase. pK_a of the catalytic cysteine and the role of the conserved histidine in a plant polyketide synthase, *J. Biol. Chem. 275*, 39640−39646.
37. Zhang, Z. Y., and Dixon, J. E. (1993) Active site labeling of the *Yersinia* protein tyrosine phosphatase: the determination of the pK_a of the active site cysteine and the function of the conserved histidine 402, *Biochemistry 32*, 9340−9345.
38. Rodrigues-Lima, F., and Dupret, J. M. (2002) In silico sequence analysis of arylamine *N*-acetyltransferases: evidence for an absence of lateral gene transfer from bacteria to vertebrates and first description of paralogs in bacteria, *Biochem. Biophys. Res. Commun. 293*, 783−792.
39. Guo, Z., Vath, G. M., Wagner, C. R., and Hanna, P. E. (2003) Arylamine *N*-acetyltransferases: Covalent modification and inactivation of hamster NAT1 by bromoacetamido derivatives of aniline and 2-aminofluorene, *J. Protein Chem. 22*, 631−642.
40. Vernet, T., Tessier, D. C., Chatellier, J., Plouffe, C., Lee, T. S., Thomas, D. Y., Storer, A. C., and Menard, R. (1995) Structural and functional roles of asparagine 175 in the cysteine protease papain, *J. Biol. Chem. 270*, 16645−16652.
41. Hengge, A. C., and Hess, R. A. (1994) Concerted or stepwise mechanism for acyl transfer reactions of *p*-nitrophenyl acetate? Transition states from isotope effects, *J. Am. Chem. Soc. 116*, 11256−11263.
42. Hess, R. A., Hengge, A. C., and Cleland, W. W. (1998) Isotope effects on enzyme-catalyzed acyl transfer from *p*-nitrophenyl acetate: concerted mechanism and increased hyperconjugation in the transition state, *J. Am. Chem. Soc. 120*, 2703−2709.

BI0497244